Structural, electronic, and optic properties of $In_2O_3(ZnO)_n$ system

Yanfa Yan, Aron Walsh, Juarez L. F. Da Silva, Su-Huai Wei, and Mowafak Al-Jassim

National Renewable Energy Laboratory, Golden, CO 80401, USA

ABSTRACT

The structural, electronic, and optic properties of the $In_2O_3(ZnO)_n$ system are studied by the combination of high-resolution electron microscopy, image simulation, and density-functional theory calculation. We find that the $In_2O_3(ZnO)_n$ system has a polytypoid structure that consists of wurtzite $InZn_nO_{n+1}$ slabs separated by single In–O octahedral layers. These octahedral layers are inversion domain boundaries and satisfy the electronic octet rule. The $InZn_nO_{n+1}$ slabs contain another type of boundary that inverts the polarities again. This boundary prefers a zigzag modulated structure and also obeys the electronic octet rule. We also found that the red-shift in optical transitions for the $In_2O_3(ZnO)_n$ system as compared to individual In_2O_3 and ZnO systems is because the symmetry-forbidden band-edge transitions found in In_2O_3 are overcome by the formation of the superlattices, with ZnO contributions to the top of the valence band. We further find that the increasing n results in an enhanced valence-band maximum in the ZnO region, while the conduction-band minimum becomes more localized on the InO2 layers, which introduces confinement to electron carriers. Such enhanced localization explains why Zn-rich compounds (higher n) exhibit lower conductivity.

1. Introduction

Transparent and conductive oxide (TCO) films have been studied extensively because they are critical components of transparent electrodes in optoelectronic devices such as flat-panel displays, solar cells, and gas sensors [1-4]. Although Sn-doped In_2O_3 (ITO) is the prototype n-type TCO (due to its superior low resistivity and high visible transparency), the high cost of indium is directing the search toward materials with reduced indium content. This situation, along with the possibility of discovering new material compositions with superior properties, has led to the investigation of ternary and quaternary systems. Recently, the $In_2O_3(ZnO)_n$ (IZO) system has become a particular focus of attention because it has shown great electrical and optical properties and also exhibits excellent chemical stability. The IZO system contains slabs of wurtzite (WZ) ZnO structure and layers of In_2O_3 bixbyite structure. As the coordination preferences in these two structures are largely maintained in the crystalline IZO system, the electronic behavior of the system would be expected for the ternary oxides. However, this is not the case. For instance, the reduction of the IZO optical bandgaps much below that of ZnO (3.44 eV) and In_2O_3 (3.75 eV), i.e., in the range of 2.9−3.1 eV for n = 2−5, is unexpected. More interestingly, the IZO amorphous phase exhibited even better electrical properties than its crystalline counterpart.

In this talk, we summarize our recent results on the atomic structure, formation mechanism, and electronic and optic properties of the IZO system studied by the combination of high-resolution electron microscopy, image simulation, and density-functional theory (DFT) calculation [5]. Our results explain well the experimentally observed phenomena.

2. Method

We performed the calculations using the density-functional theory, as implemented in the VASP code, with local density approximation. The energy cutoff for the plane-wave expansion was 400 eV. In all calculations, all the atoms are allowed to relax until the Hellmann-Feynman forces acting on them become less than 0.02 eV/Å. For optical and electronic calculation, the In and Zn d states were treated as valence within the projector augmented wave method. Exchange and correlation effects were treated by a hybrid HSE approach in which a percentage of exact Fock-exchange is added to the PBE functional and a screening of $\omega = 0.11$ bohr^{-1} is applied. At this level, the calculated bandgaps for ZnO and In_2O_3

are 3.39 and 2.74 eV, respectively. The layered In-modulated IZO structures employed ($R\bar{3}m$ derived symmetry) were taken from recent DFT calculations. There are 4, 6, and 10 formula units for the n = 1, 3, and 5 structures, respectively. A k-point grid density of 4×4×2 was used for n = 1, with similar quality meshes for higher n. Electron diffraction and high-resolution transmission electron microscopy (HRTEM) simulations were carried out using the MacTempas program. The optical parameters of the microscope used for the simulations were a spherical aberration coefficient Cs = 1.0 mm and a beam convergence semiangle of a = 0.5 mrad.

3. Results

Figure 1(a) shows the atomic structure of flat-layer $In_2O_3(ZnO)_6$, which is often proposed for $In_2O_3(ZnO)_n$ in the literature. The structure is projected along the $[11\bar{2}0]$ zone axis of the ZnO structure. The c-axis is vertical. It shows the feature that two In-O octahedral layers sandwich a WZ $InZn_nO_{n+1}$ slab. ZnO possesses a WZ structure with polarity along its c-axis. Here, we define the positive polarity as the direction from O to Zn along the c-axis, as indicated by the large arrows. An In-O octahedron is indicated by "Oct." The In atoms (marked by In1) in the octahedral layers are six-fold coordinated by O atoms. The inversion character is clearly observed. The polarities of ZnO at two sides of an In-O octahedral layer are inverted. The polarity in the side above the In-O octahedral layer points up, whereas the polarity in the side below this layer points down. Thus, the In-O octahedral layers give a tail-to-tail polarity configuration. Furthermore, another boundary in the $InZn_nO_{n+1}$ slab is required to invert the polarity again to form a head-to-head configuration, as indicated by the large arrows. The flat second polarity-inversion boundary with trigonal bipyramid structure has long been considered as the model for the IZO system. However, it is not consistent with HRTEM images, which have shown that the IZO systems exhibit modulated structure with dark zigzag contrast in the $InZn_nO_{n+1}$ slabs.

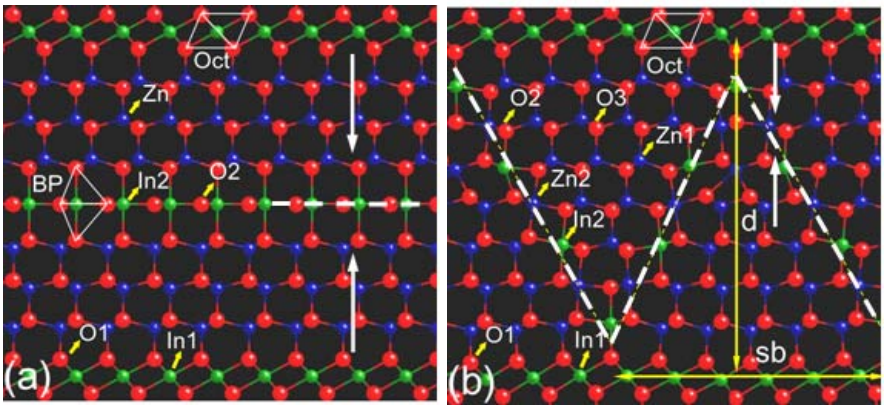

Figure 1. Structure models for IZO systems with (a) flat boundary and (b) zigzag boundary in the (Zn/In)-O slab.

Figure 1(b) shows our proposed modulated structure for the second polarity-inversion boundary. Unlike in Fig. 1(a), our new structure not only satisfies the In-O octahedron rule, but it also satisfies the modulation rule. The boundary in the ZnO slab is now located along the zigzag dashed lines. In this model, the O atoms on the boundary are four-fold coordinated and In and Zn atoms are five-fold coordinated. The modulated boundary provides the second polarity inversion (head-to-head configuration). The distance (d) between the In-O octahedral layers determines the overall composition (the number n) and the width of the modulation (sb). To see the relative stability, we performed total-energy calculations for the two structures shown in Figs. 1(a) and 1(b). Both structures are fully relaxed. We find that the total energy of the modulated structure shown in Fig. 1(b) is 4.24 eV lower than that of the structure with the flat-layer In-O boundary shown in Fig. 1(a). We find that there are two main reasons why the flat boundary is not energetically favorable. First, the flat In-O layer inside the ZnO

slab is highly mismatched with ZnO, causing considerable strain around the In-O layer. This strain is significantly reduced in the modulated structure, as In and Zn atoms arrange alternatively. Second, O atoms are three-fold coordinated in the flat In-O layer, which is energetically unfavorable. In the modulated structure, all O atoms in the zigzag boundary are four-fold coordinated, which is energetically more favorable. These two changes gain significant energies. Thus, the second polarity-inversion boundary inside $InZn_nO_{n+1}$ layers prefers the modulated structure.

The calculated local electronic density of states (DOS) of IZO are shown in Fig. 2. The distribution of states is similar to that expected from a combination of ZnO and In_2O_3, i.e., there is a Zn d band at the bottom of the upper valance band (VB) that hybridizes with O p located at the top of the VB. As the In 4d states lie to higher binding energy (−13.5 eV) than Zn 3d (−5.5 eV), they make a weaker contribution to the valence states (via reduced p − d coupling). The distribution of In states from the InO_2 octahedra and mixed In/Zn layers is similar, except for hybridization of the mixed ions with Zn at −6 eV. The lower conduction band (CB) contains contributions from In, Zn, and O s; the delocalized nature of the CB minimum state for n = 1 can be observed in Fig. 2. For higher values of n, the DOS features remain unchanged, except for the increased contribution of the ZnO framework to the VB and In to the CB. The predicted Γ-point HSE bandgaps are 2.91, 3.04, and 3.05 eV for n = 1, 3, and 5, respectively. These offer substantial improvement over PBE alone (2.0−2.3 eV lower), and reproduce the monotonic increase empirically observed with higher n.

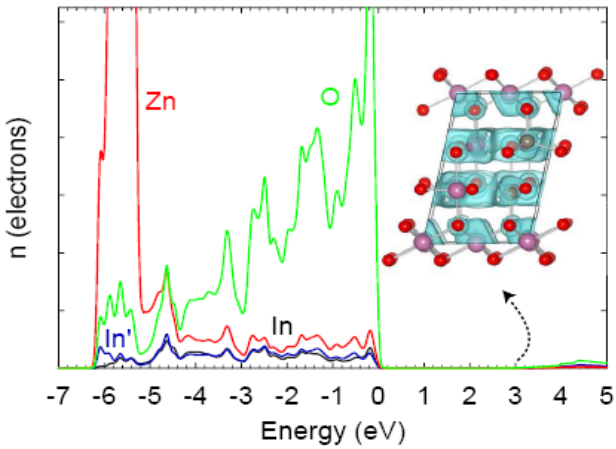

Figure 2. Local electronic density of states of $In_2O_3(ZnO)$, with an isosurface of the conduction-band minimum state plotted at 1 me/Å^3 (inset). 'In' refers to In atoms in the InO_2 octahedron, while 'In' refers to In atoms in the mixed In/Zn layers.

The decomposition of the band-edge states in IZO (Fig. 4) reveals that the VB maximum arises from the Zn−O networks, i.e., from Zn d − O p hybridization, while the CB minimum is a hybridized mixture of In, Zn, and O s states. The transitions from the VB to CB extrema result in allowed optical matrix elements (> 0.7 a.u.) for all values of n. The band-edge states from the ZnO layers now contribute to strong optical absorption.

Figure 3 shows the calculated band structures, which can be used to interpret the electronic behavior of the IZO compounds. The top of the VB exhibits no significant dispersion, indicating a large barrier for hole mobility. In contrast, the CB is highly dispersed. For larger values of n, the effects of band folding can be observed. The spatial distribution of the CB states is critical in determining the n-type mobility and subsequent conductivity. Isosurfaces of the CB minimum states are also shown in Fig. 5. For n = 1, only two mixed cation layers are present between the In octahedra, and these contain equal contributions from In and Zn, which results in an electron distribution spread over the entire cell (similar to a homogeneous alloy). For n = 3 and 5, the number of intermixed layers increases to 4 and 6, respectively, and with the increased Zn concentration, a more effective superlattice is formed. Here, the

carriers become more confined in the InO_2 octahedron networks; however, the modulated In ions in the ZnO layers make a significant additional contribution to the CB in n = 3 and 5, as observed from the electron density distribution in Fig. 3. Overall, the inhomogeneity of the CB states for larger n diminishes the isotropy of the conduction network, which will, in turn, result in greater barriers to n-type conductivity. This correlates with the minimum in resistivity reported for IZO samples with low Zn concentrations, i.e., $0 < n < 1$.

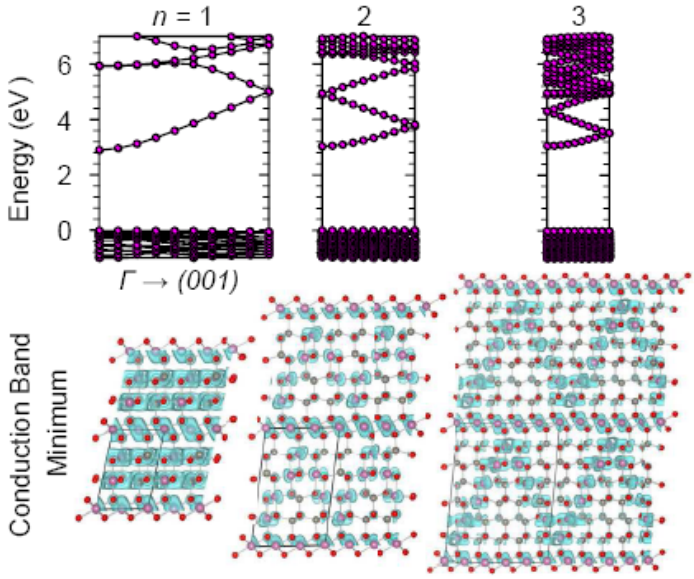

Figure 3. $In_2O_3(ZnO)_n$ band dispersions along $\frac{2\pi}{a}$ (001), with isosurfaces of the corresponding conduction-band minimum state plotted at 1 me/Å^3 (inset).

4. Conclusion

In summary, we have studied the atomic structure, formation mechanism, electronic, and optic properties of the IZO system by the combination of high-resolution electron microscopy, image simulation, and density-functional theory calculation. We found that the structure of the ITO system satisfies the following: the octahedron rule for the InO_2 layer, the inversion domain boundary, stacking faults, and modulation rules for the $InZn_nO_{n+1}$ slabs, and electronic octet rule for O atoms in the $InZn_nO_{n+1}$ layers. We further find that the increasing n results in an enhanced valence-band maximum in the ZnO region, while the conduction-band minimum becomes more localized on the InO_2 layers, which introduces confinement to electron carriers. Such enhanced localization explains why Zn-rich compounds (higher n) exhibit lower conductivity. Our results explain well the experimentally observed phenomena.

5. References

[1] D.S. Ginley and C. Bright, *MRS Bull.* **25,** 15 (2000).
[2] I. Hamberg, C. G. Granqvist, K. F. Berggren, B. E. Sernelius, and L. Engstrom, *Phys. Rev. B* **30**, 3240 (1984).
[3] P. D. C. King, T. D. Veal, D. J. Payne, A. Bourlange, R. G. Egdell, and C. F. McConville, *Phys. Rev. Lett.* **101**, 116808 (2008).
[4] A. Walsh, J. L. F. Da Silva, S.-H. Wei, et al., *Phys. Rev. Lett.* **100**, 167402 (2008).
[5] Y. Yan, J. L. F. Da Silva, S.-H. Wei, and M. Al-Jassim, *Appl. Phys. Lett.* **90**, 261904 (2007); J. L. F. D. Silva, Y. Yan, and S.-H. Wei, *Phys. Rev. Lett.* **100**, 255501 (2008).